Tropical Cyclone Simulations with the Betts Convective Adjustment Scheme. Part I: Model Description and Control Simulation

JONG-JIN BAIK

Department of Marine, Earth, and Atmospheric Sciences, North Carolina State University, Raleigh, North Carolina

MARK DEMARIA

Hurricane Research Division, AOML/NOAA, Miami, Florida

SETHU RAMAN

Department of Marine, Earth, and Atmospheric Sciences, North Carolina State University, Raleigh, North Carolina

(Manuscript received 10 March 1989, in final form 2 August 1989)

ABSTRACT

A new convective parameterization scheme proposed by Betts is tested in a tropical cyclone model. The convective adjustment scheme adjusts the local temperature and moisture structures towards the observed quasi-equilibrium thermodynamic state and includes nonprecipitating shallow convection as well as deep convection. The numerical model used for this study is an axisymmetric, primitive equation, hydrostatic, finite difference model with 15 vertical levels and a horizontal resolution of 20 km. The spectral radiation boundary condition, which uses a different gravity wave speed for each vertical mode, is implemented in the model.

It is shown that the convective scheme is capable of simulating the developing, rapidly intensifying, and mature stages of a tropical cyclone from a weak vortex. At the mature stage, the minimum surface pressure and maximum low level tangential wind speed are around 923 mb and 58 m s^{-1}. During the early developing stage, the latent heat release is from the convective parameterization, but at the mature stage the latent heat release is mainly due to the grid-scale phase change.

For comparison, an experiment is conducted with the parameterized convection excluded, leaving only the grid-scale condensation and evaporation. The results show that the development of a tropical cyclone can be modeled with crude grid-scale condensation and evaporation processes for the 20 km horizontal resolution, similar to other studies. However, the storm with the explicit convective latent heat release is considerably less intense than that with the parameterized convective latent heat release.

1. Introduction

The genesis, intensification, and maintenance of tropical cyclones have been studied widely during the past three decades because of their spectacular nature in the atmosphere. Many observational and theoretical studies (e.g., Riehl and Malkus 1961; Charney and Eliassen 1964) have indicated that the energy which drives the system comes from the latent heat release in deep cumulus clouds. The complex interaction between the cumulus convection and the larger-scale circulation makes tropical cyclone research a difficult task.

To investigators who work with numerical models, a tolerable substitute for the observed cumulus clouds is required. Since the horizontal dimensions of convective elements are on the order of 0.1–10 km, explicit treatment of convective motions may be possible with models that have horizontal grid intervals on this order or less. With this approach, cumulus parameterization is bypassed and the closure is moved down from the cloud-scale circulation to the in-cloud turbulence and cloud physics (Ooyama 1982). Research along this line can be found in either hydrostatic (Rosenthal 1978; Jones 1980) or nonhydrostatic (Yamasaki 1977; Willoughby et al. 1984; Rotunno and Emanuel 1987) tropical cyclone models, although horizontal resolution near the storm center varies considerably from 0.4 km (Yamasaki) to 20 km (Rosenthal).

On the other hand, the main research direction in the problem of organized cumulus convection has been to regard convective processes as subgrid-scale phenomena, which cannot be resolved by the model. Cumulus parameterization schemes currently being used in large- and mesoscale models can be categorized into three groups: the moisture convergence scheme (Kuo 1965, 1974), the Arakawa–Schubert scheme (1974), and the moist convective adjustment scheme (Manabe

Corresponding author address: Dr. Sethu Raman, Dept. of Marine, Earth, and Atmospheric Sciences, North Carolina State University, Raleigh, NC 27695-8208.

et al. 1965). Detailed descriptions of these schemes can be found in a review by Frank (1983).

The moisture convergence scheme, commonly referred to as the Kuo scheme, assumes that the moisture supply by large-scale convergence and evaporation from the surface sustains penetrative cumulus convection. Because of its simplicity and the close link between large-scale moisture convergence and convection, it is very popular in tropical cyclone models (see Anthes 1982, Table 4.1.). The specification of moisture partitioning is one of the problems of the Kuo scheme and several methods have been proposed for this purpose (e.g., Anthes 1977; Geleyn 1985).

The Arakawa–Schubert scheme describes the mutual interaction of a cumulus cloud ensemble with the large-scale environment and uses the quasi-equilibrium hypothesis, which means that the cumulus ensemble follows a sequence of quasi-equilibria with the large-scale forcing. This is the most elegant scheme to date and gives a clear physical picture of the interaction between the cumulus clouds and their environment. However, its complicated formulation makes it difficult to implement in numerical models and it is computationally expensive. Because of this, only a few studies (Wada 1979; Hack and Schubert 1980) have used this method to simulate tropical cyclones.

The moist convective adjustment scheme assumes that in the presence of deep convection, the local thermodynamic structure is adjusted towards the quasi-equilibrium state and uses a moist adiabatic equilibrium structure as a reference. In Kurihara and Tuleya's (1974) three-dimensional tropical cyclone model, cumulus convection was treated with this concept.

The main disadvantage of the moist convective adjustment scheme is that the tropical atmosphere does not approach a moist adiabatic equilibrium state in the presence of deep convection. Thus, Betts (1986) proposed a new convective adjustment scheme that relaxes the vertical temperature and moisture fields towards observed quasi-equilibrium thermodynamic structures. Two separate schemes are used for deep and shallow convection. Although the Betts scheme does not explain the detailed physical interaction between the cloud and its environment, it will give more realistic convective heating and moistening in the vertical because of the use of reference profiles based on observations. In fact, preliminary studies (Betts and Miller 1986) with the incorporation of this scheme into the ECMWF global forecast model showed a significant improvement in the tropical mean flow compared with the operational Kuo scheme.

Stimulated by the above result, we adopt the Betts scheme to represent the collective effect of cumulus convection and investigate the development of tropical cyclones through numerical simulations with an axisymmetric model. Although some minor modifications have been made to the scheme (Betts 1989, personal communication), the version described by Betts (1986) will be used in this study. A description of the model is given in section 2. In section 3, cumulus parameterization for deep and shallow convection is described. Results of a control simulation are presented in section 4 and it is shown that the model can produce a tropical cyclone from a weak vortex.

2. Description of the numerical model

a. Governing equations

The formulation of governing equations in the present model is the same as that of Hack and Schubert (1980, hereafter HS). The equation set is written with axisymmetric polar coordinates in the horizontal and σ-coordinate in the vertical on an f-plane. The σ-coordinate is defined by

$$\sigma \equiv \frac{p - p_T}{p_S - p_T} \equiv \frac{p - p_T}{\pi}, \tag{2.1}$$

where p is the pressure, p_T the pressure at the model top, p_S the surface pressure, and $\pi \equiv p_S - p_T$. The p_T is specified as 50 mb for the present study. The upper and lower boundary conditions are given by $\dot{\sigma} = 0$ at $\sigma = 0$ and 1 where $\dot{\sigma}$ is the vertical σ-velocity $d\sigma/dt$. The law of conservation of momentum yields the radial momentum equation, the tangential momentum equation, and the vertical momentum equation, which is assumed to be hydrostatic. These are given by

$$\frac{\partial}{\partial t}(\pi r u) = -\frac{\partial}{\partial r}(\pi r u u) - \frac{\partial}{\partial \sigma}(\pi r \dot{\sigma} u) + \left(f + \frac{v}{r}\right)\pi r v - r\left(\pi \frac{\partial \phi}{\partial r} + \sigma \pi \alpha \frac{\partial \pi}{\partial r}\right) + \pi r D_u, \tag{2.2}$$

$$\frac{\partial}{\partial t}(\pi r v) = -\frac{\partial}{\partial r}(\pi r u v) - \frac{\partial}{\partial \sigma}(\pi r \dot{\sigma} v) - \left(f + \frac{v}{r}\right)\pi r u + \pi r D_v, \tag{2.3}$$

$$\frac{\partial \phi}{\partial \sigma} = -\pi \alpha, \tag{2.4}$$

respectively. Here, t is the time, r the radius in polar coordinates, u the radial wind component, v the tangential wind component, f the Coriolis parameter, ϕ the geopotential, and α the specific volume for air. The last terms in (2.2) and (2.3) represent the frictional forces due to the diffusion of momentum. The mass continuity equation combined with the upper and lower boundary conditions is

$$\frac{\partial}{\partial t}(\pi r) = -\frac{\partial}{\partial r}\int_0^1 \pi r u d\sigma. \tag{2.5}$$

The vertical σ-velocity is

$$\dot{\sigma} = -\frac{1}{\pi r}\left[\sigma \frac{\partial}{\partial t}(\pi r) + \frac{\partial}{\partial r}\int_0^\sigma \pi r u d\sigma'\right]. \tag{2.6}$$

The thermodynamic energy equation and continuity equation for water vapor are

$$\frac{\partial}{\partial t}(\pi r T) = -\frac{\partial}{\partial r}(\pi r u T) - \left(\frac{p}{p_0}\right)^{\kappa}\frac{\partial}{\partial \sigma}(\pi r \dot{\sigma}\theta) + \frac{\pi r \sigma \alpha}{c_p}\left(\frac{\partial}{\partial t} + u\frac{\partial}{\partial r}\right)\pi + \pi r \frac{L}{c_p}(C - E) + \pi r D_T + \pi r Q_R + \pi r F_T, \quad (2.7)$$

$$\frac{\partial}{\partial t}(\pi r q) = -\frac{\partial}{\partial r}(\pi r u q) - \frac{\partial}{\partial \sigma}(\pi r \dot{\sigma} q) + \pi r(E - C) + \pi r D_q + \pi r F_q, \quad (2.8)$$

respectively. Here, T is the temperature, θ the potential temperature, p_0 the reference pressure (=1000 mb), L the latent heat of evaporation, c_p the heat capacity for air at constant pressure, $\kappa \equiv R/c_p$, where R is the gas constant for air, and q the mixing ratio of water vapor. The C and E terms represent grid-scale condensation and evaporation processes and Q_R represents radiative processes. The D_T and D_q terms represent diffusion of temperature and water vapor. The F_T and F_q in (2.7) and (2.8) represent the effect of heating and moistening associated with cumulus convection, respectively. The cumulus effect will be parameterized in section 3. Equations (2.1)–(2.8), the equation of state, and the definition of potential temperature yield ten equations in the ten unknown variables. Table 1 shows the independent, prognostic, and diagnostic variables that appear in the governing equations.

b. Subgrid-scale diffusion

The subgrid-scale horizontal diffusion of momentum, heat, and water vapor is calculated in the manner given by HS. The lateral eddy diffusion coefficient is expressed as the sum of linear and nonlinear terms. The appropriate value of the linear term is chosen from the analysis of a linearized tangential momentum equation. The nonlinear term is treated by the nonlinear viscosity scheme proposed by Smagorinsky (1963). The lateral eddy diffusion coefficient of heat and water vapor is assumed to be the same as that of momentum.

The vertical diffusion of momentum, heat, and water vapor is included by using the eddy diffusion coefficient method. The vertical eddy diffusion coefficient for momentum K_m is given by

TABLE 1. The independent, prognostic, and diagnostic variables that appear in the governing equations.

Independent	Prognostic	Diagnostic
t	u	p
r	v	$\dot{\sigma}$
σ	π	α
	T	ϕ
	q	θ

$$K_m = 1 + l_V^2\left[\left(\frac{\partial u}{\partial z}\right)^2 + \left(\frac{\partial v}{\partial z}\right)^2\right]^{1/2}, \quad (2.9)$$

where l_V is a constant vertical mixing length and z the height. The value of 30 m is chosen for l_V, which corresponds to the mixing length for the neutral condition in Kurihara and Tuleya's (1974) model. The diffusion coefficient of heat K_h and water vapor K_q is related to that of momentum by $K_h = K_q = 3K_m$ (Klemp and Wilhelmson 1978; Willoughby et al. 1984). This relationship is valid in neutral and unstable conditions (Deardorff 1980).

The air–sea exchange processes of momentum, heat, and water vapor are parameterized by the bulk aerodynamic method. The exchange coefficients for momentum, heat, and water vapor are considered to be equal. For the given height and magnitude of the model-produced lowest level vector wind, the 10 m height wind speed and drag coefficient are iteratively computed assuming that the lowest level wind is in the constant stress layer (see Kondo 1975).

c. Radiation

Although the diabatic heating rate due to radiative processes is smaller than that due to cumulus convection, several numerical studies (e.g., Sundqvist 1970; Kurihara and Tuleya 1981) indicate that differential radiative cooling makes an important contribution to a storm development in the early stage. The differential cooling gives a favorable condition for convection by enhancing baroclinicity and driving radial-vertical flows (secondary circulations). Moreover, the longwave radiational cooling near the cloud top has an effect of destabilization and helps the growth of convective clouds in the upper portion of a storm. Sundqvist included the radiative cooling effect by applying a vertical profile of infrared cooling only to regions where condensation is not taking place. Kurihara and Tuleya included the effect of radiational heating or cooling by specifying the vertical structures of temperature and mixing ratio to a typical condition in the tropics and considering only the existence or nonexistence of condensation at each level. Following HS, in this study two vertical profiles (convectively disturbed and convectively suppressed) of net radiative cooling rates are used from the GATE (GARP Atlantic Tropical Experiment) radiation data analysis (Cox and Griffith 1979). When the convective adjustment scheme selects a deep convection calculation at a grid point, the convectively disturbed profile is used. Otherwise, the convectively suppressed profile is used. At the uppermost model integer level (level 1), which lies in the stratosphere, the radiational data are not available. Newtonian cooling is applied at that level using

$$Q_R = -\frac{\theta - \theta_0}{\tau_R}, \quad (2.10)$$

where θ_0 is the initial potential temperature and τ_R is a relaxation time scale for radiational cooling. This relaxes the temperature at level 1 towards the initial state. The τ_R is set to 12 hours (Rotunno and Emanuel 1987). The radiational scheme in (2.10) is included to smooth temperature fields near the model top. The radiation parameterization does not include the diurnal cycle, which has been used by Hobgood (1986).

d. *Grid-scale phase change and dry convective adjustment*

If in the course of integration the air is found to be supersaturated at a grid point, grid-scale condensation, evaporation, and precipitation processes are allowed. The excess water vapor is condensed to liquid water and latent heat release follows. Then, the liquid water is considered to precipitate into the layer immediately below and completely evaporate. When this brings that layer to supersaturation, the process is repeated. An excess is precipitated as rain onto the surface when the lowermost layer is reached. The above procedure is the same as that developed for the UCLA general circulation model (Arakawa et al. 1974).

When absolutely unstable layers exist, we eliminate them using dry convective adjustment. This is a substitute for the free convection process in which condensation is not involved (Kurihara and Tuleya 1974). The procedure is identical to that for the UCLA general circulation model (Arakawa et al. 1974). The computation is repeated until the temperature stratification becomes stable in the entire column of air.

e. *Numerical solution*

The model atmosphere consists of 15 layers. The integer level is located in each layer and bounded by the half-integer levels. Table 2 shows the 15 integer levels and approximate corresponding pressure levels assuming that p_S = 1008.7 mb. This value is used for the initial surface pressure at the model lateral boundary. The prognostic variables u, v, T, q are defined at the integer levels, while $\dot{\sigma}$ is defined at the half-integer levels. The size of the horizontal domain is 1000 km with equally spaced grid intervals of 20 km. The horizontal grid system is staggered with the Arakawa B scheme in which the variables u, v are placed at the half-integer positions and the variables π, T, q at the integer positions. Our spatial finite difference approximations for the governing equations follow those given by HS. The diffusion and radiative terms are time-integrated with the forward difference scheme; other terms with the leapfrog scheme. The time step is 30 sec. The Asselin (1972) time filter is used to prevent time separation of the solutions and the horizontal space smoothing of fourth-order diffusion form is applied to all the prognostic variables in order to reduce the high-frequency noise. An 8-day integration of the numerical model required about 9 minutes of computing time on the Naval Research Laboratory's Cray XMP.

TABLE 2. The integer σ levels and approximate corresponding pressure levels assuming that p_s = 1008.7 mb.

Level index	σ	Pressure (mb)
1	0.0209	70
2	0.0522	100
3	0.1043	150
4	0.1565	200
5	0.2086	250
6	0.2608	300
7	0.3651	400
8	0.4694	500
9	0.5737	600
10	0.6780	700
11	0.7823	800
12	0.8345	850
13	0.8866	900
14	0.9482	960
15	0.9805	990

f. *Boundary and initial conditions*

In the tropical atmosphere, most of the available potential energy generated by the latent heat release is partitioned to outward propagating gravity-inertia waves (Schubert et al. 1980). It is therefore very important to minimize the possible influence of the lateral boundaries on solutions. Primitive equation tropical cyclone models have generally used a large domain to reduce the effect of lateral boundaries [e.g., 2500 km in Wada's (1979) axisymmetric model]. Hack and Schubert (1981) designed a radiation boundary condition that uses a different gravity wave speed for each vertical mode. This radiation boundary condition is implemented in the model so that a domain size of 1000 km can be used.

The initial conditions of the five prognostic variables π, u, v, T, q are needed for the time integration. An assumption is made that π, v, and ϕ fields are initially in gradient wind balance with zero radial wind. Therefore, if the initial tangential wind profile and lateral boundary values of surface pressure and temperature are specified, we can compute the initial surface pressure and temperature fields using the hydrostatic and gradient wind equations. The structure of the initial tangential wind is given by

$$v = v_m\left[\frac{2(r/r_m)}{1+(r/r_m)^2}\right]\left[\frac{3(\sigma/\sigma_m)}{2+(\sigma/\sigma_m)^3}\right], \quad (2.11)$$

where v_m, r_m, and σ_m are specified as 7 m s^{-1}, 210 km, and 0.9, respectively. Equation (2.11) gives a maximum tangential wind of 7 m s^{-1} at $r = r_m$ and $\sigma = \sigma_m$. At the lateral boundary, the initial temperature is given according to the mean tropical clear areas sounding in the western Pacific (Gray et al. 1975) and the initial

surface pressure is 1008.7 mb. The above procedure yields a maximum temperature difference of 0.7°C at the 0.4694 σ-surface between the center and the boundary and a minimum surface pressure of 1004.9 mb. The initial relative humidity field is obtained from the mean tropical cluster environment profile in the western Pacific (Gray et al. 1975). In addition, a Gaussian type perturbation with the amplitude of 10% and e-folding radius of 200 km is added to the moisture field near the disturbance center in order to reduce the integration time before storm development occurs. For the simulations, the sea surface temperature is set to 28°C and the Coriolis parameter is evaluated at 20°N.

3. Cumulus parameterization with a convective adjustment scheme

Convective adjustment schemes employ the concept that in the presence of cumulus convection the local thermodynamic structures are constrained by the convection and adjusted towards a quasi-equilibrium reference state. So, the convective heating and moistening terms in (2.7) and (2.8) can be parameterized as

$$F_T = \frac{T_{\text{ref}} - \bar{T}}{\tau}, \tag{3.1}$$

$$F_q = \frac{q_{\text{ref}} - \bar{q}}{\tau}, \tag{3.2}$$

respectively. Here, the subscript ref denotes the reference state and the overbar the grid point value before convection. The factor τ is the adjustment time scale, or relaxation time scale. Thus, the convective parameterization problem consists of determining a criterion to determine when the adjustment scheme is activated, the adjustment time scale, and the reference thermodynamic profiles.

Before the convective adjustment is taken into consideration, the grid-scale condensation and evaporation processes and the dry convective adjustment described in section 2d have already removed the grid-scale supersaturation and absolutely unstable situations, respectively. Therefore, the convective scheme is applied to a conditionally unstable atmosphere with relative humidity less than 100%. An experiment was performed where the convective scheme was applied before the grid-scale phase change processes and the results were almost identical. Thus, the order of the application of the grid-scale and convective-scale schemes does not appear to be important.

The unstable layers are found by the check of positive buoyancy as follows. Consider a hypothetical parcel along a moist adiabat, which is constructed using the saturation point (temperature and pressure at the lifting condensation level) of the lowermost model integer level (= level 15). If a lifted parcel along this moist adiabat is not buoyant at level 13 with respect to the environmental (grid point) temperature sounding, the convective scheme is skipped at that grid point. Otherwise, the cloud top is computed as the last level before the moist adiabat crosses the vertical profile of the environmental temperature and the convective scheme is applied. For the present tropical cyclone model, we simply specify cloud base as level 14. However, cloud base level could be calculated if the vertical resolution of the model were fine enough in the lower atmosphere. The buoyancy test is not made at levels 15 and 14.

The relaxation time scale represents the lag between the large-scale forcing and the convective response. Betts and Miller (1986, hereafter BM) tested the effect of changing the adjustment time scale with a single column model and showed that a time scale of 2 hours gives the best reproduction of the structures of the mean GATE wave. This model also uses a specified value.

The essence of the convective parameterization given by Betts (1986) lies in the construction of the reference profiles. Different convective regions may have different quasi-equilibrium thermodynamic states, which can be documented observationally. An advantage of the scheme is that the parameters; e.g., relaxation time scale, saturation pressure departure etc., can be easily tuned by comparison with observations.

We can conceptually divide cumulus clouds into precipitating (deep convection) and nonprecipitating (shallow convection). Shallow clouds generally have cloud top heights less than 3 km and do not involve a net latent heat release when averaged over their lifetime (Frank 1983). The parametric basis of the deep convection is therefore quite different from that of the shallow convection. Deep and shallow convection is initially separated by the cloud top level. If the computed cloud top height is above level 11 height, we select the deep convection scheme. Otherwise, the shallow convection scheme is applied.

a. Deep convection

Observational studies, including composite typhoon sounding, in the tropical regions (Betts 1986) revealed that in the presence of penetrative cumulus convection a quasi-equilibrium temperature structure below the freezing level parallels a moist virtual adiabat, isolines of constant virtual equivalent potential temperature (θ_{ESV}), rather than a moist adiabat (θ_{ES}) and above the freezing level it shows a gradual increase of θ_{ES} towards the θ_{ES} adiabat established using a saturation point at a low level. A rising saturated parcel along a moist virtual adiabat has the buoyancy correction for cloud water. An increase of θ_{ES} above the freezing level is probably related to the increase of cloud parcel buoyancy due to the freezing of cloud water and the fallout of precipitation. As a parametric basis for deep convection, we simply assign a reference temperature profile with a minimum θ_{ES} at the freezing level by considering the moist virtual adiabatic equilibrium struc-

ture as a reference thermodynamic state in the lower troposphere. Accordingly, the reference thermal profile in the lower troposphere is more unstable than the moist adiabat. The deep convection scheme adjusts from below cloud base, so that it can simulate the effect of cold unsaturated downdrafts.

The reference potential temperature gradient up to the freezing level is given by

$$\left(\frac{\partial\theta}{\partial p}\right)_{\text{ref}} = w\left(\frac{\partial\theta}{\partial p}\right)_m, \tag{3.3}$$

where w is a stability weight on the moist adiabat in the lower troposphere and subscript m means that the quantity in parentheses is evaluated on the moist adiabatic isoline. Thus, a first-guess reference potential temperature profile is established by

$$\theta_{\text{ref}}(p) = \theta_{\text{ref}}(p^-) + w\left(\frac{\partial\theta}{\partial p}\right)_m (p - p^-), \tag{3.4}$$

where p^- is the pressure level just below the level on which $\theta_{\text{ref}}(p)$ is computed. The θ_{ref} at level 15 is potential temperature at that level.

From above the freezing level to the cloud top, a first-guess reference potential temperature profile is constructed by

$$\theta_{\text{ref}}(p) = \theta_m(p) - \frac{a(p - p_t) + b(p_f - p)}{p_f - p_t}, \tag{3.5}$$

where

$$a = \theta_m(p_f) - \theta_{\text{ref}}(p_f), \tag{3.6a}$$

$$b = \theta_m(p_t) - \bar{\theta}(p_t). \tag{3.6b}$$

Here, p_f and p_t are pressure levels at the freezing level and cloud top, respectively. The θ_m is potential temperature on the moist adiabat, which is constructed using a saturation point [see (3.7)] at level 15. The profile (3.5) gives an increase of reference potential temperature back to the environmental potential temperature at cloud top. In the finite-layer numerical model, the potential temperature at cloud top, $\bar{\theta}(p_t)$, is usually not equal to the $\theta_m(p_t)$ because cloud top level is enforced to be on the model level.

The moisture reference profile is established using a saturation pressure departure parameter S, which is defined as

$$S \equiv p^* - p, \tag{3.7}$$

where p is the pressure at a particular level and p^* is the pressure at which an air parcel would become saturated if moved adiabatically. The parameter S is a measure of subsaturation, so it controls relative humidity during the adjustment. The value of saturation pressure departure at any pressure level is found by specifying S at the lowermost model integer level (denoted by S_a) and two constant slopes n_1 and n_2. Up to the freezing level, the profile S is given by

$$S(p) = S_a\left(1 + n_1 \frac{p_a - p}{p_a - p_f}\right), \tag{3.8}$$

and from above the freezing level to the cloud top, it is expressed by

$$S(p) = S_a\left(1 + n_1 - n_2 \frac{p_f - p}{p_f - p_t}\right), \tag{3.9}$$

where p_a is pressure at level 15. For the present study, a negative value of S_a (unsaturated) is chosen. Two slope constants are specified as $n_1 = 0.25$ and $n_2 = 0.5$, so that the saturation pressure departure is greatest at the freezing level. The allowance for the maximum absolute value of S at the freezing level gave a good reproduction of GATE wave data (BM). The first-guess reference mixing ratio follows from

$$q_{\text{ref}} = q(T^*, p^*), \tag{3.10}$$

where $T^* = T_{\text{ref}}(p^*/p)^\kappa$ and $p^* = S + p$ from (3.7). The q_{ref} is approximated using the mixing ratio formula and the Teten's formula which give

$$q_{\text{ref}} = \frac{379.91}{p^*} \exp\left[\frac{c_1(T^* - 273.16)}{T^* - c_2}\right]. \tag{3.11}$$

Here, c_1 and c_2 are constants ($c_1 = 17.269$, $c_2 = 35.86$).

The above procedure provides first-guess reference thermodynamic structures. These are then adjusted using the iterative procedure described by Betts (1986) to ensure that moist static energy will be conserved. Two iterations were found to be sufficient to satisfy the constraint.

Once the reference profiles are determined, the subgrid-scale convective precipitation rate PR is calculated by

$$\text{PR} = \frac{1}{g}\int_{p_a}^{p_t}\left(\frac{q_{\text{ref}} - \bar{q}}{\tau}\right)dp, \tag{3.12a}$$

or

$$\text{PR} = -\frac{c_p}{gL}\int_{p_a}^{p_t}\left(\frac{T_{\text{ref}} - \bar{T}}{\tau}\right)dp, \tag{3.12b}$$

where g is gravity. If the computed convective precipitation is negative, cloud top is specified as level 11 and shallow convection scheme is selected. In the presence of weak subsidence, this situation is possible.

b. Shallow convection

Observational studies in the tropics (Betts 1986) showed that the quasi-equilibrium thermodynamic structure in the shallow convective regions tends to be close to a mixing line that connects the saturation point of air above the cloud layer and that of subcloud air.

This implies that the shallow convection is a moist mixing process which includes the subcloud layer air, the cloud layer air, and the air above cloud layer. The shallow convection scheme adjusts the levels from cloud base to cloud top and the level just above cloud top. We construct first-guess reference thermodynamic profiles and then correct them to satisfy enthalpy and moisture constraints.

A mixing structure parameter β is defined as

$$\beta \equiv \frac{dp^*}{dp}. \tag{3.13}$$

From (3.13), it follows that

$$\frac{\partial \theta}{\partial p} = \beta\left(\frac{\partial \theta}{\partial p^*}\right)_{\text{ml}}, \tag{3.14a}$$

$$\frac{\partial q}{\partial p} = \beta\left(\frac{\partial q}{\partial p^*}\right)_{\text{ml}}, \tag{3.14b}$$

where subscript ml means mixing line. The parameter β is a measure of the mixing intensity in shallow convection. For a well-mixed subcloud layer, where the potential temperature and mixing ratio are nearly constant with height, β approaches zero. When β is equal to one, the θ and q profiles are parallel to a mixing line. The layer with $\beta < 1$ has a thermodynamic structure characterized by the potential temperature and mixing ratio profiles converging towards a mixing line. On the other hand, the layer with $\beta > 1$ corresponds to a structure with θ and q profiles diverging from a mixing line. The inversion layer; e.g., trade wind inversion, has a value of $\beta > 1$. From cloud base to cloud top, the mixing structure parameter β is specified as 1 for the present study. In the layer just above cloud top, β is calculated with the requirement that $1 \leqslant \beta \leqslant 2.5$ for a smooth transition across the inversion. A mixing line slope, denoted by M, is computed using saturation points at level 15 and at the second level above cloud top, which is not modified by the shallow convection scheme. Since the thickness between cloud top and the second level above cloud top is larger than 100 mb in the present model, the saturation point structure in that layer is typically too stable. The shallow cloudy planetary boundary layer is destabilized radiatively (Betts 1983). Because of these, a modified mixing line slope M_α is introduced where

$$M_\alpha = \alpha M, \tag{3.15}$$

and α is a stability weight on the mixing line slope. Choosing a value of $\alpha < 1$ corresponds to the destabilization of the mixing line. For the present simulations, α is set to 0.8. Using β and M_α, a first-guess reference potential temperature profile is obtained by using the relation

$$\theta_{\text{ref}}(p) = \theta_{\text{ref}}(p^-) + \beta M_\alpha (p - p^-). \tag{3.16}$$

At cloud base level, θ_{ref} is assigned to the grid point potential temperature. The value of the saturation pressure departure parameter at any level is calculated using (3.7) and (3.13) and is given by

$$S(p) = S(p^-) + (\beta - 1)(p - p^-). \tag{3.17}$$

In the case of $\beta = 1$, the saturation pressure departure parameter S is constant in the shallow cloud layer. In the cloud layer, a value of $S = -30$ mb is given. Then, a first-guess reference mixing ratio is computed by (3.10), (3.11) and (3.17).

For the shallow convection, the reference profiles are adjusted so that enthalpy and moisture are conserved. This implies that heat and moisture are simply redistributed in the vertical.

4. Control simulation

For a control experiment with the convective parameterization scheme described in section 3, we specify three undetermined convective parameters as follows. The adjustment time scale τ is set to 2 hours for both deep and shallow convection. The stability weight on the moist adiabat in the lower troposphere w in the deep scheme is specified as 0.95. Since the moist virtual adiabat has a slope of about 0.9 times that of a moist adiabat (Betts 1986), a value of 0.95 gives a slope about halfway between that of a moist and a moist virtual adiabat. The saturation pressure departure at the lowermost model integer level S_a in the deep adjustment scheme is set to -30 mb. This gives saturation pressure departure values of -37.5 and -22.5 mb at freezing and cloud top levels, respectively. These and other assigned values in section 3 were chosen intuitively from the previous studies on the thermodynamic structure of tropical cyclones by many researchers and the preliminary results of the global model forecasting with the Betts scheme by BM, rather than from analyzing composite tropical cyclone sounding data in detail. The sensitivity to these parameters is described in Part II.

The time evolution of the minimum surface pressure and maximum low level (level 15) tangential wind speed is shown in Figs. 1a and 1b. This figure indicates that the model with the new convective adjustment scheme is capable of simulating a tropical cyclone from an initial weak vortex. The intensification rate of the model storm in terms of the minimum surface pressure is very slow for the first 48 hours and increases slightly for the next 48 hours. During the period 96–144 h, the storm grows very rapidly and after 144 h it is nearly in a steady state. For the one day period starting at 108 h, the pressure drops by about 40 mb. This very rapid decrease during a short time period is often observed in nature (e.g., Willoughby et al. 1982). The intensification in terms of the maximum low level tangential wind speed is similar to that of the minimum surface pressure. Based on the results shown in Fig. 1, we define a mature stage as the period between 144 and 192 h

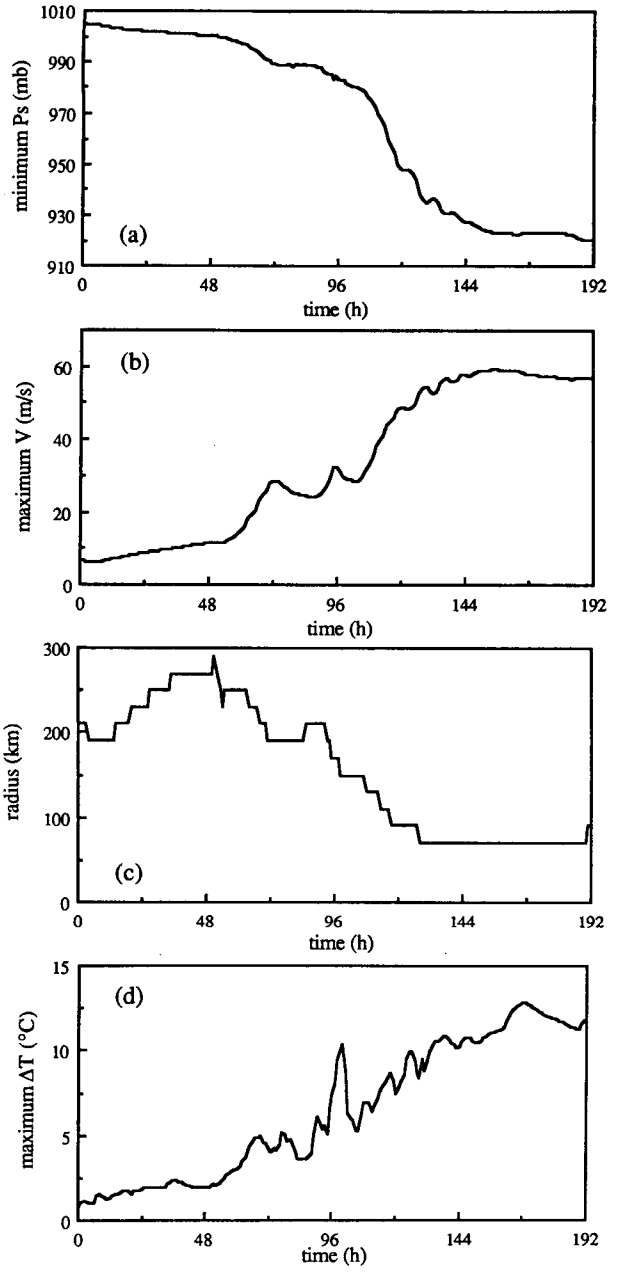

FIG. 1. (a) The time evolution of the minimum surface pressure, (b) the maximum low level tangential wind speed, (c) the radius of the maximum low level tangential wind speed, and (d) the maximum temperature deviation from the model lateral boundary for the control experiment.

for the subsequent analyses. At the mature stage, the minimum surface pressure and maximum low level tangential wind speed are around 923 mb and 58 m s^{-1}.

The radius of the maximum low level tangential wind speed is shown in Fig. 1c. It is initially located at 210 km. A general trend is that it moves gradually outward up to 51 h and then inward until 128 h. After that time, it reaches a constant value of 70 km. Fig. 1d shows the time evolution of the maximum temperature deviation from the model lateral boundary. The magnitude of the warm core increases after 48 h with a maximum temperature deviation of 12.9°C at 168 h.

The initial model environment is a crucial factor for the evolution of the model storm. Rotunno and Emanuel (1987) noticed that the average sounding in the tropics during the summer; e.g., Jordan's (1958) sounding which was widely used in tropical cyclone modeling research, is nearly neutral to actual clouds while the numerical model's version of clouds may grow rapidly in the same situation. In their study, this artificial conditional instability, which can sometimes result in very rapid development of an initial storm, was removed by creating an initial state that is neutral to the model's clouds. There is a small amount of convective instability in the model initial condition used here since the initial reference profile near the storm center is slightly warmer than the model temperature profile. However, Fig. 1 shows that the model storm does not intensify until after 48 h and that the rapid intensification does not occur until after 96 h. This suggests that the initial convective instability is not a serious problem.

Figure 2 shows the time evolution of the inner 500 km domain-averaged total, grid-scale, and convective precipitation rates. The total (grid-scale plus convective) precipitation rate gradually increases during the first 2 days and then oscillates during the next 4 days.

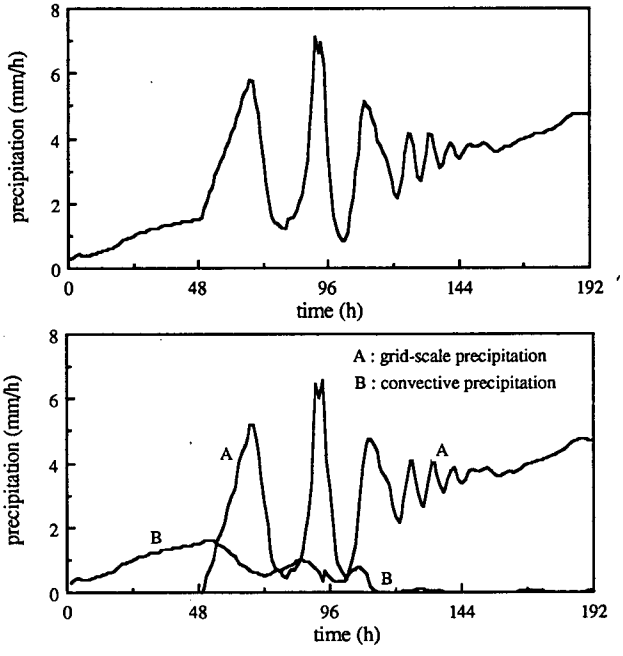

FIG. 2. The time evolution of the inner 500 km domain-averaged total precipitation rate (upper panel) and grid-scale and convective precipitation rates (lower panel) for the control experiment.

At the mature stage, the precipitation rate slowly increases until the end of the time integration. The lower panel of Fig. 2 shows that for the first 48 hours, the diabatic heating is from the subgrid-scale deep cumulus convection, while after about 110 h it is primarily from the grid-scale phase change. From 48 to about 110 h, there is a transition from subgrid-scale to grid-scale precipitation. Figure 2 also shows that the oscillation in the time history of the total precipitation rate is due to the grid-scale precipitation. Comparing Fig. 2 with Fig. 1 shows that the oscillations in the grid-scale heating result in oscillations in the maximum low level tangential wind.

The oscillations in the grid-scale heating appear to be related to the assumption that the excess liquid water, which results from supersaturation, falls into the layer below and evaporates until that layer becomes saturated. When all of the liquid water is assumed to evaporate, many layers can become saturated without any net release of latent heat. Eventually, the lowest layers become saturated and the net latent heat rapidly increases. This rapid change in the latent heating (with a lower level maximum) appears to cause the oscillation in Fig. 2. This hypothesis was tested by performing a simulation where all of the excess liquid water that results from supersaturation was assumed to immediately fall out as rain. In this case, the magnitude of the oscillation in the grid-scale heating was reduced, and the maximum grid-scale heating occurred at a higher vertical level. It would probably be advantageous to design a grid-scale scheme that allowed some fraction of the liquid water to evaporate into the next lower layer. The two extremes discussed above allow all or none of the liquid water to be evaporated.

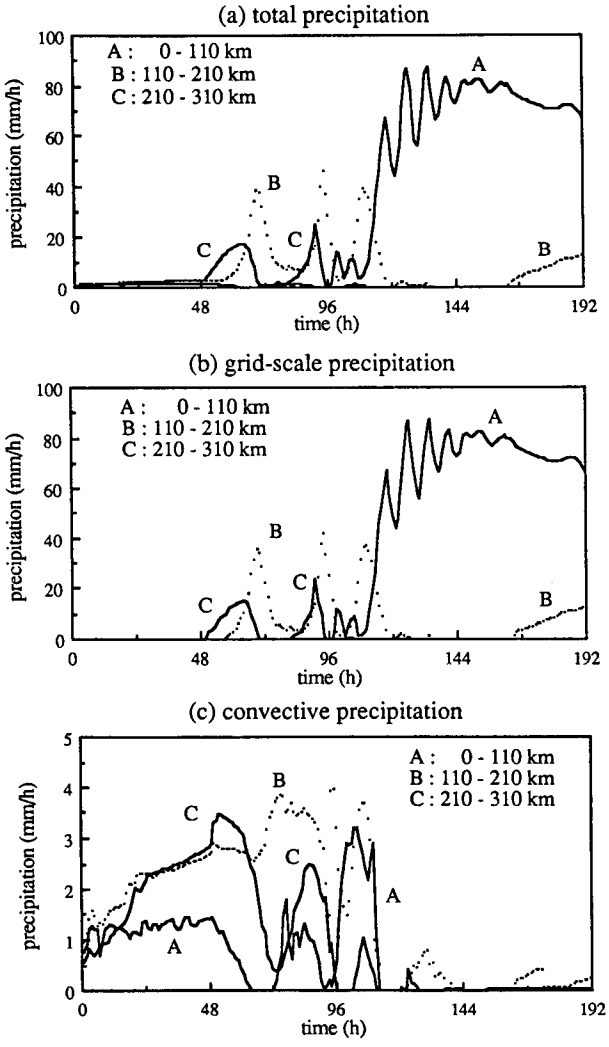

FIG. 3. (a) The time evolution of the 0–110 km, 110–210 km, and 210–310 km band averaged total, (b) grid-scale, and (c) convective precipitation rates for the control experiment.

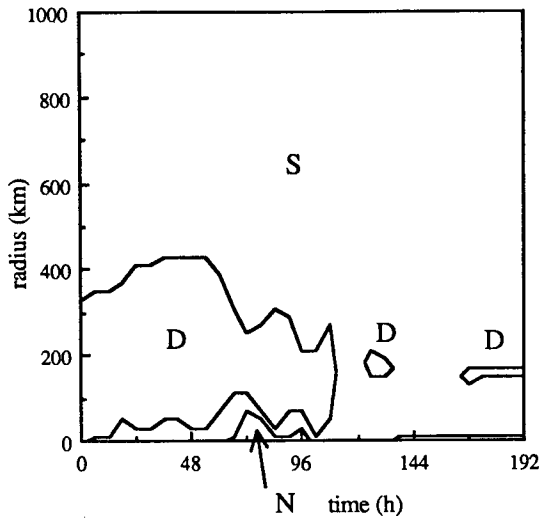

FIG. 4. The time evolution of the radial intervals where the deep convective, shallow convective, or no-convective adjustment schemes are applied. The letters D, S, and N indicate the deep, shallow, and no-convections, respectively.

To investigate the radial dependency of the precipitation, the time history of the 0–110 km (A), 110–210 km (B), 210–310 km (C) band averaged total, grid-scale, and convective precipitation rates are presented in Fig. 3. In area C, the rainfall continues up to around 96 h. Afterward, the rainfall becomes confined to area A. This implies that the maximum precipitation zone, hence the strong heating zone, is shifted inward as the storm develops. At the mature stage, the average precipitation rate in area A is around 75 mm h^{-1}. The radial dependency of the grid-scale precipitation is very similar to that of the total precipitation.

Figure 4 shows the time evolution of the radial intervals where the deep convective, shallow convective, or no-convective adjustment schemes are applied. Shortly after the time integration starts, the deep convection occupies the area within 330 km radius. The

radial interval which contains the deep clouds increases until 54 h, rapidly shrinks for the next 18 hours, exhibits some oscillations, and vanishes around at 110 h. The shallow convection is present in the area beyond 430 km radius through the entire time integration period. After about 110 h, the model domain is occupied by the shallow clouds except at one or two grid points, which still have deep clouds. Up to around 110 h, an area where shallow convective or no-convective adjustment schemes are applied is observed in the inner region of the domain. Thus, the rapid intensification period shown in Fig. 1 is associated with the grid-scale rather than the convective-scale heating.

Because the deep convective heating region becomes very small after about 96 h, the radiational cooling profile for the convectively suppressed case is being applied over most of the domain. In an actual storm, there would probably be a cirrus shield as well as stratiform clouds, so the convectively suppressed profile is probably not appropriate. It would probably be better to include the vertically integrated moisture in the determination of the cooling profiles, or to use a more general radiation scheme. However, as will be shown in Part II, the radiation scheme only has a small effect on the mature stage of the storm.

The vertical convective heating profiles at 20, 100, 200, 300 and 500 km radii at 24, 48, 72 and 96 hours are shown in Fig. 5. At 20 km, the shallow convection exists at 24 and 48 h and the overall heating structure is similar to that predicted with the Betts scheme using the ATEX (Atlantic Trade Wind Experiment) and BOMEX (Barbados Oceanographic and Meteorological Experiment) datasets (BM). The convective cooling just above the shallow cloud top represents the evaporation of overshooting shallow cloud tops. The shallow convection at this radius is destroyed at 72 and

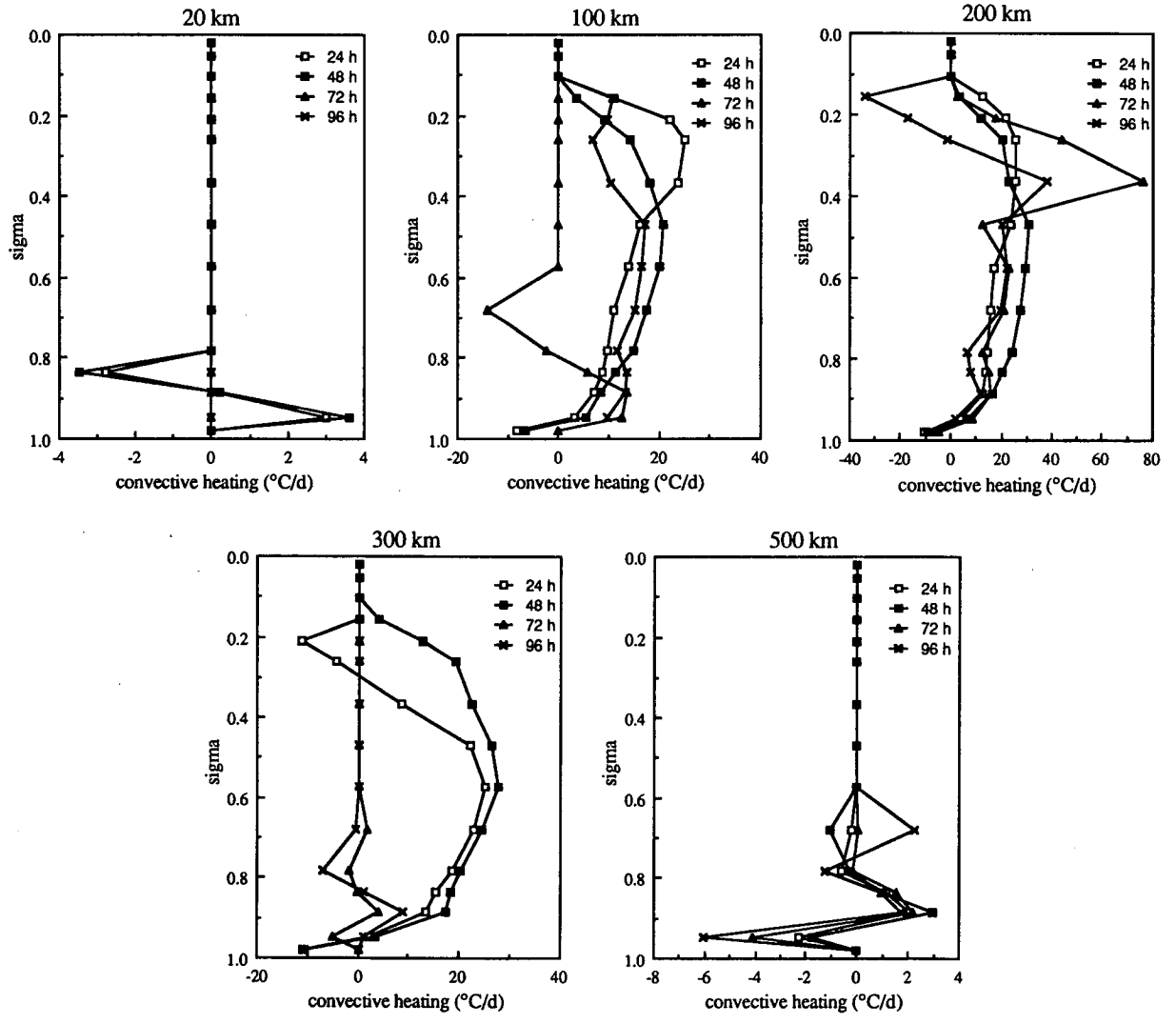

FIG. 5. The vertical convective heating profiles at different radii at several times.

96 h. At 100 km, the maximum heating zone in the vertical is located in the upper troposphere at 24 h and moves to the mid-troposphere at 48 h. The shallow convection is present at 72 h. The shallow clouds grow into the deep clouds and the deep convection exists at 96 h. At 200 km, during the period between 24 and 48 h the level of maximum convective heating zone shifts downward, similar to the profile at 100 km radius. There is strong cooling below the deep cloud top at 96 h. At 300 km, the deep convective heating rate increases from 24 to 48 h, and then deep convection becomes shallow convection at 72 and 96 h. At 500 km, the shallow convection occurs during the entire time period, although the structure of the vertical convective heating changes slightly with time. The top of the shallow cloud at 500 km is located at a higher level than that at 20 km. The lower shallow cloud top at 20 km is associated with the strong subsidence near the storm center.

Figure 5 showed the diversity of the convective heating profiles, which depend on the evolution of the model storm at various locations. Some of the deep convective heating profiles, like those at 24 h, 48 h, 96 h at 100 km; at 24 h, 48 h at 200 km; and at 48 h at 300 km, are comparable to heating profiles deduced from observational and theoretical studies (see Chang 1976, Fig. 1). On the other hand, the deep heating profiles with cooling near the cloud top, like those at 96 h at 200 km and at 24 h at 300 km, can usually only be obtained by employing sophisticated cumulus parameterization schemes (e.g., Fritsch and Chappell 1980a,b).

For the analyses of the dynamic and thermodynamic structures of the mature model tropical cyclone, a time stage of 168 h is selected. The radius–height cross sections of the tangential, radial, and vertical wind speeds at 168 h are presented in Fig. 6 and the cross sections of the temperature deviation from the value at the model lateral boundary and the relative humidity at 168 h are shown in Fig. 7. In these figures, only the inner 500 km domain is shown for increased resolution.

The tangential wind field exhibits the cyclonic circulation throughout the entire model atmosphere inside a radius of about 450 km. Beyond that, the anticyclonic circulation in the upper portion of the atmosphere extends outward with a maximum value of -20 m s^{-1} at 970 km radius and level 3. The radius of the maximum tangential wind increases with height in the lower and middle troposphere. It is 70 km at level 15 and 130 km at level 7. Although the location of the maximum wind speed in the model occurs at a larger radial distance from the center than in actual tropical cyclones (e.g., Jorgensen 1984), the outward tilts of the maximum wind speed and vertical motion in the eyewall (see Fig. 6) are observed in nature (e.g., Jorgensen 1984) and are also consistent with the modeling study of Willoughby et al. (1984). The larger radius of the maximum wind is probably related to the coarse horizontal resolution of the present numerical model.

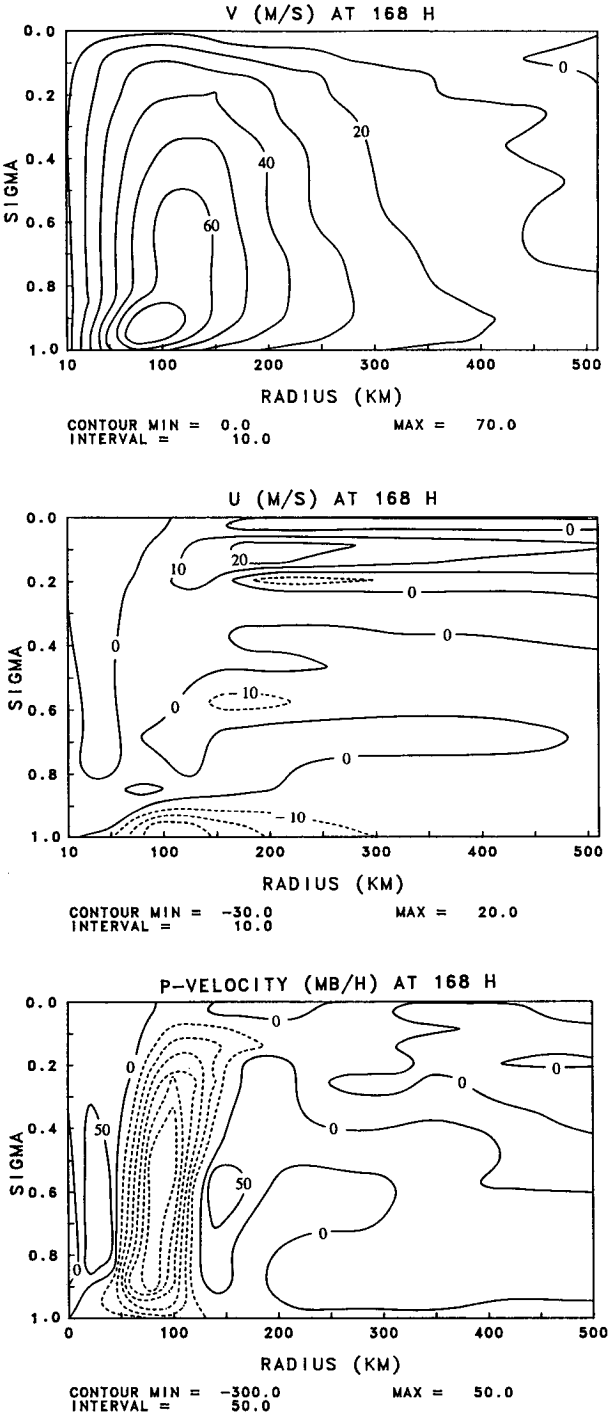

FIG. 6. The radius–height cross section of the tangential wind speed, radial wind speed, and vertical p-velocity at 168 h for the control experiment.

The radial wind field shows strong inflow in the lower levels with its maximum value located at level 15,

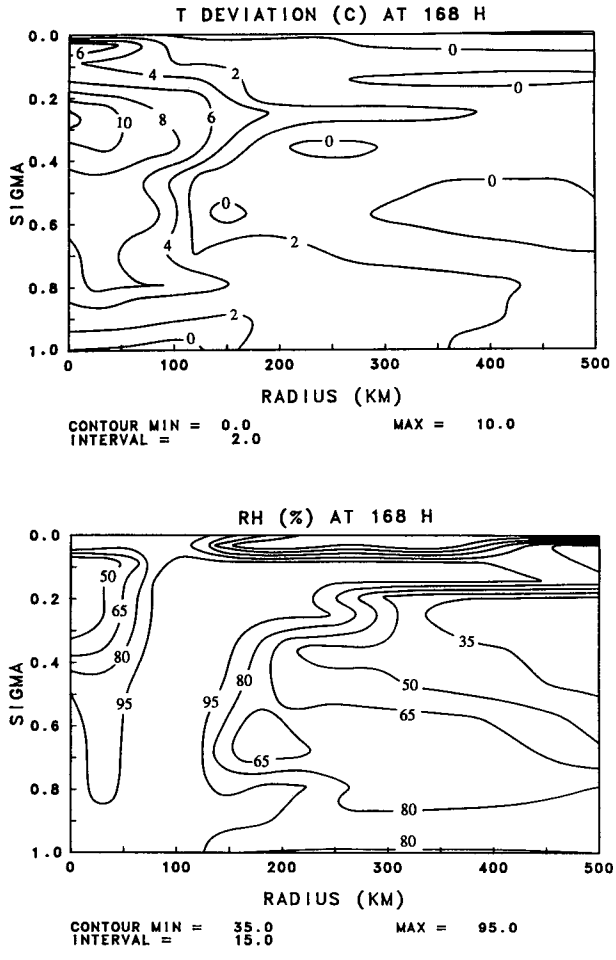

FIG. 7. The radius–height cross section of the temperature deviation and relative humidity at 168 h for the control experiment.

which implies that it is mainly frictionally driven. There is an outflow jet centered near level 3 and a shallow inflow zone just below the outflow jet. Another area of radial inflow, which is surrounded by relatively weak outflows, is found near level 9. There is a weak inflow region near the storm center, which corresponds to an area of downward motion, as is seen in the vertical velocity cross section in Fig. 6. The vertical motion field is characterized by subsidence in a well-defined eye, a strong eyewall updraft with a slight outward tilt, and subsidence just outside of the eyewall. The magnitude of the compensating mesoscale downdraft just outside of the eyewall seems to be large compared with other studies (e.g., Kurihara and Tuleya 1974). This downdraft, however, can play an important role in preventing the model storm from further development through low level drying outward from the eyewall (Fig. 7).

The temperature deviation field shows a warm region near the center with a maximum located at level 6. The relatively cool region at levels 14 and 15 inside of 150 km radius is a result of adiabatic cooling of air flowing towards the low pressure center. The relative humidity field shows a moist region associated with the eyewall and outflow jet and a dry zone related to the eye. A broad dry region exists below outflow jet and above approximately level 10 beyond about 200 km. A similar dry region was reported by other numerical studies (e.g., Rosenthal 1978). There is also a relatively dry region at low levels outside of the eyewall, which was present in several modeling studies (Rosenthal 1978; Jones 1980; Rotunno and Emanuel 1987). In that region, the relative humidity at level 15 is lower than that at level 14, implying that the vertical mixing tends to homogenize the potential temperature and mixing ratio in the planetary boundary layer (Anthes and Chang 1978).

The tropical ocean is a reservoir of energy that feeds a tropical cyclone. The interaction between the model storm and the ocean occurs by the differences between the atmospheric variables at the 10 m level and the corresponding values at the sea surface. Figure 8 shows the time evolution of the inner 500 km domain-averaged drag coefficient, surface stress, sensible heat flux, and latent heat flux for the control experiment. The domain-averaged drag coefficient gradually increases from 1.15×10^{-3} to about 1.75×10^{-3} at the mature stage. Rotunno and Emanuel (1987) reported that with a constant drag coefficient of 1.1×10^{-3} the transfer rate of moist entropy from the sea surface is too small to obtain a tropical cyclone in a reasonable time, and with a constant value of 3.0×10^{-3} the transfer rate is too large for the outer regions of the vortex and hence distorts the moist entropy budget in the boundary layer. Thus, the inclusion of drag coefficient as a function of wind speed as described in section 2b gives reasonable values of the drag coefficient.

The pattern of the time evolution of the domain-averaged surface stress in Fig. 8 is similar to that of the drag coefficient since both are closely linked to the wind speed at 10 m level. The calculated value at 168 h is 1.05 N m^{-2}. This value is close to the values at 60 and 120 km in a steady-state model hurricane (Anthes and Chang 1978). Note that our model tropical cyclone at the mature stage is stronger than one simulated by Anthes and Chang.

The domain-averaged sensible heat flux in Fig. 8 is upward (positive) up to 64 h and then downward, except for a short period between 105 and 107 h, until the end of the time integration. The downward sensible heat flux at a steady-state has been found by previous studies (Kurihara 1975; Anthes and Chang 1978; Rotunno and Emanuel 1987). Anthes and Chang (1978) argued that in order to maintain an isothermal planetary boundary layer at a steady state there must be a net downward entrainment of the air above the planetary boundary layer with higher potential temperature. Further analyses on the direction of sensible heat flux at 100, 300, 500, 700 and 900 km radii during the mature stage (not shown here) show that the sensible

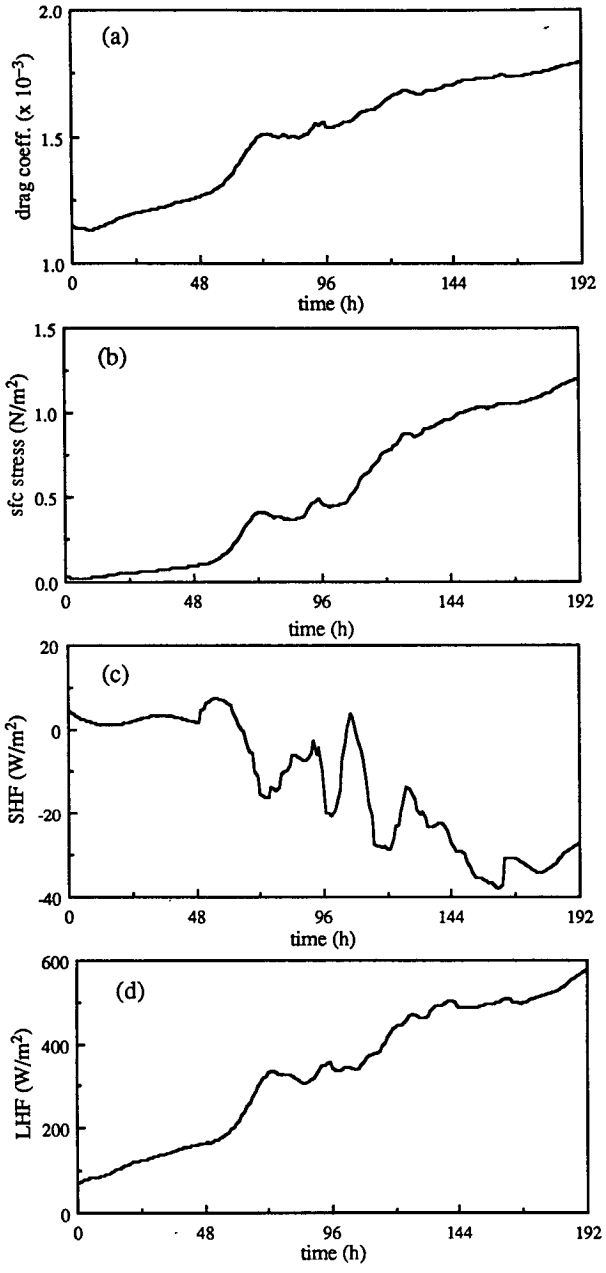

FIG. 8. (a) The time evolution of the inner 500 km domain-averaged drag coefficient, (b) surface stress, (c) sensible heat flux, and (d) latent heat flux for the control experiment.

heat flux is downward at 300 and 500 km and upward at other locations. The upward sensible heat flux at 100 km, which is greater than that at 700 and 900 km, is attributed to the compensation for the adiabatic cooling of air flowing in towards the low pressure center, noting that the horizontal surface pressure gradient at 100 km is much greater than that at 300 and 500 km. The pattern of the time history of the domain-averaged latent heat flux is also similar to that of the drag coefficient. The amount of the calculated latent heat flux is much larger than that of the computed sensible heat flux, in agreement with many other studies.

In a steady-state model hurricane, as a first approximation, precipitation is balanced by evaporation from the sea surface and horizontal transport of water vapor across a vertical wall (Anthes and Chang 1978). At the mature stage, the inner 500 km domain-averaged precipitation rate and latent heat flux from the ocean are about 4 mm h^{-1} and 510 W m^{-2}, respectively. From these two values, the estimate of the horizontal transport of water vapor across the wall at 500 km is about 0.91 g m^{-2} s^{-1}, which is equivalent to the energy flux of 2275 W m^{-2}. Thus, the ratio of the evaporation to the horizontal transport of water vapor is 0.22. This ratio is comparable to the values computed from the observations and modeling results (see Anthes 1982, Table 3.1.). For example, from the water vapor budget analysis of the model hurricane in the radial ring of 0–500 km, Kurihara (1975) obtained a ratio of 0.26.

To further study the variation of latent heat flux, the time evolution of the latent heat flux at 100, 300 and 500 km radii together with the variation of corresponding drag coefficient is shown in Fig. 9. The overall patterns are very similar. This figure indicates that latent heat flux near the storm center at the mature stage is very high compared with that at the other locations. At the mature stage, the computed drag coefficient at 100 km ($\sim 3.3 \times 10^{-3}$) is 2.0 and 2.3 times

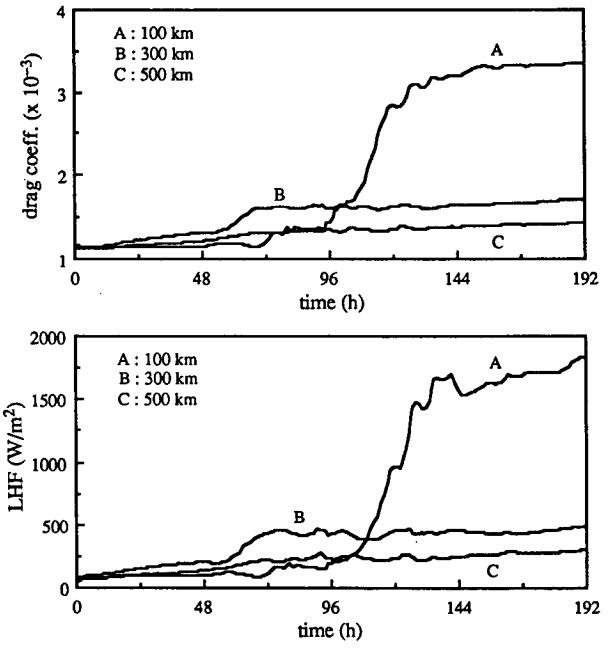

FIG. 9. The time evolution of the drag coefficient (upper panel) and latent heat flux (lower panel) at different radii for the control experiment.

larger than that at 300 and 500 km and the calculated latent heat flux at 100 km ($\sim$1680 W m^{-2}) is 3.7 and 6.1 times greater than that at 300 and 500 km.

As described in the Introduction, there have been several studies that simulate tropical cyclones without parameterized convection. A common factor in models with convection explicitly resolved is the inclusion of a liquid water prediction equation with the sophisticated cloud microphysics. However, HS performed several numerical experiments in which the parameterized convection with the Arakawa–Schubert scheme was excluded, leaving the mechanism of latent heat release to the grid-scale (15 km horizontal resolution) condensation and evaporation processes. In the treatment of grid-scale condensation and evaporation processes, HS followed the approach developed for the UCLA general circulation model (Arakawa et al. 1974) and adopted in the present model. Even though HS used crude grid-scale condensation and evaporation processes, they could simulate development of a tropical cyclone. From these results, HS concluded that the results presented by Rosenthal (1978) are not very sensitive to the technique employed to represent the process of latent heat release.

An experiment is conducted with the parameterized convection excluded, leaving only the grid-scale condensation and evaporation. Figure 10 shows the time evolution of the minimum surface pressure and maximum low level tangential wind speed for this case. This figure shows that the development of a tropical cyclone can be modeled with crude grid-scale condensation and evaporation processes for the 20 km horizontal resolution and supports the conclusion by HS. Comparing Figs. 1 and 10, it can be seen that the model storm with the parameterized convective latent heat release becomes much more intense than that with the explicit latent heat release. Thus, although the subgrid-scale precipitation becomes negligible at the mature stage, it still has a large effect on the storm intensity when the mature stage is reached.

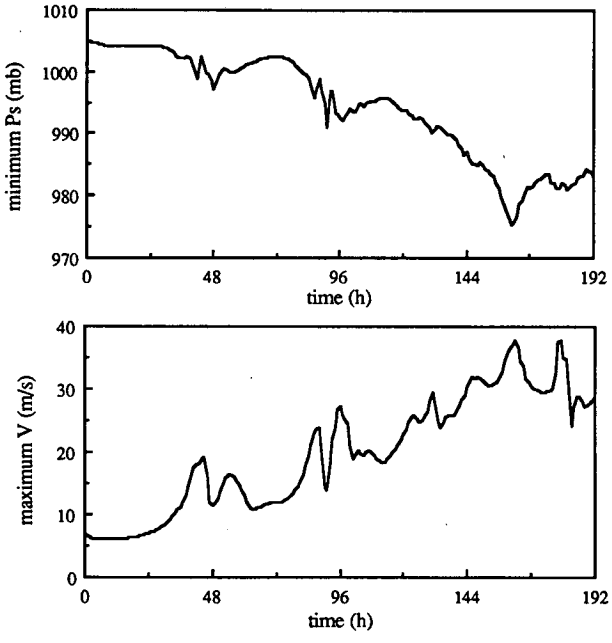

FIG. 10. The time evolution of the minimum surface pressure (upper panel) and the maximum low level tangential wind speed (lower panel) for the experiment with the parameterized cumulus convection excluded.

The fact that the model storm with the convective heating is much more intense at the mature stage than the storm without the convective heating is somewhat surprising. In the control simulation, the contribution of the convective heating to the total heating becomes very small after about 96 h when the storm begins to intensify rapidly. Thus, it might be expected that the storm structure at the mature stage would be independent of the convective heating. However, an examination of the storm structure during the first 4 days of the integration showed that there were large differences between the simulations with and without the convective heating, which then affected the subsequent rapid intensification period. As described previously, the grid-scale heating tends to produce a vertical heating profile with a maximum in low levels. Without the convective heating, the vortex tends to spin up rapidly in low levels. By 96 h, the maximum tangential wind is about 35 m s^{-1} and decreases rapidly with height above the 500 mb level. When the convective heating is included, the tangential wind decreases more slowly with height so that tangential winds exceeding 20 m s^{-1} extend all the way up to about 150 mb. Thus, it appears that the vortex structure at 96 h in the simulation with the convective heating is more favorable for continued intensification.

5. Summary

A new convective adjustment scheme, which allows for nonprecipitating shallow convection as well as deep convection, proposed by Betts (1986) was incorporated into a tropical cyclone model. The numerical model is an axisymmetric, primitive equation, hydrostatic, finite difference model with 15 vertical levels and a horizontal resolution of 20 km. The model contains subgrid-scale horizontal and vertical diffusion, air–sea interaction, simple radiation, grid-scale phase change, dry convective adjustment, and subgrid-scale cumulus convection processes. A horizontal domain size of 1000 km could be used by implementing the spectral radiation boundary condition (Hack and Schubert 1981), which uses a different gravity wave speed for each vertical mode. The convective parameterization scheme is based on the concept that in the presence of cumulus convection the local temperature and moisture structures are constrained by convection and adjusted towards a quasi-equilibrium reference state where the

reference state is based on observations. The new scheme is attractive because it is simple, but gives realistic vertical heating and moistening due to cumulus convection by relaxing the atmospheric state to observed thermodynamic structures.

The results of a control simulation showed that the scheme can simulate the developing, rapidly intensifying, and mature stages of a tropical cyclone from a weak vortex. As the storm intensifies, the latent heat release by the parameterized convection decreases and at the mature stage the latent heat release is mainly from the grid-scale phase change.

The model was integrated with the parameterized convection excluded, leaving the mechanism of latent heat release to the grid-scale condensation and evaporation. The results indicated that the tropical cyclone development can be modeled with crude grid-scale condensation and evaporation processes for the 20 km horizontal resolution, similar to other studies. However, the storm with the explicit latent heat release was much less intense than in the simulation with the parameterized convective latent heat release.

The main purpose of this paper (Part I) was to investigate whether or not the new convective adjustment scheme can simulate the development of a tropical cyclone. In Part II, extensive sensitivity experiments will be carried out to study how the model storm evolution is affected by variations in the adjustment parameters, physical environment, initial conditions, and horizontal resolution.

Acknowledgments. The authors would like to thank James Hack and Alan Betts for providing valuable comments on this study. This research was supported by National Science Foundation under Grant ATM-8521611. The computer time for this research was provided by the Naval Research Laboratory.

REFERENCES

Anthes, R. A., 1977: A cumulus parameterization scheme utilizing a one-dimensional cloud model. *Mon. Wea. Rev.*, **105,** 270–286.

——, 1982: *Tropical Cyclones: Their Evolution, Structure and Effects. Meteor. Monogr.*, No. 41, Amer. Meteor. Soc., 208 pp.

——, and S. W. Chang, 1978: Response of the hurricane boundary layer to changes of sea surface temperature in a numerical model. *J. Atmos. Sci.*, **35,** 1240–1255.

Arakawa, A., and W. H. Schubert, 1974: Interaction of a cumulus cloud ensemble with the large-scale environment, Part I. *J. Atmos. Sci.*, **31,** 674–701.

——, Y. Mintz and collaborators, 1974: The UCLA atmospheric general circulation model. Dept. of Meteorology, UCLA,

Asselin, R., 1972: Frequency filter for time integrations. *Mon. Wea. Rev.*, **100,** 487–490.

Baik, J.-J., M. DeMaria and S. Raman, 1990: Tropical cyclone simulations with the Betts convective adjustment scheme. Part II: Sensitivity experiments. *Mon. Wea. Rev.*, **118,** 529–541.

Betts, A. K., 1983: Thermodynamics of mixed stratocumulus layers: Saturation point budgets. *J. Atmos. Sci.*, **40,** 2655–2670.

——, 1986: A new convective adjustment scheme. Part I: Observational and theoretical basis. *Quart. J. Roy. Meteor. Soc.*, **112,** 677–691.

——, and M. J. Miller, 1986: A new convective adjustment scheme. Part II: Single column tests using GATE wave, BOMEX, ATEX and arctic air-mass data sets. *Quart. J. Roy. Meteor. Soc.*, **112,** 693–709.

Chang, C.-P., 1976: Vertical structure of tropical waves maintained by internally-induced cumulus heating. *J. Atmos. Sci.*, **33,** 729–739.

Charney, J. G., and A. Eliassen, 1964: On the growth of the hurricane depression. *J. Atmos. Sci.*, **21,** 68–75.

Cox, S. K., and K. T. Griffith, 1979: Estimates of radiative divergence during phase III of the GARP Atlantic Tropical Experiment: Part II. Analysis of phase III results. *J. Atmos. Sci.*, **36,** 586–601.

Deardorff, J. W., 1980: Stratocumulus-capped mixed layers derived from a three-dimensional model. *Bound.-Layer Meteor.*, **18,** 495–527.

Frank, W. M., 1983: The cumulus parameterization problem. *Mon. Wea. Rev.*, **111,** 1859–1871.

Fritsch, J. M., and C. F. Chappell, 1980a: Numerical prediction of convectively driven mesoscale pressure systems. Part I: Convective parameterization. *J. Atmos. Sci.*, **37,** 1722–1733.

——, and ——, 1980b: Numerical prediction of convectively driven mesoscale pressure systems. Part II: Mesoscale model. *J. Atmos. Sci.*, **37,** 1734–1762.

Geleyn, J.-F., 1985: On a simple, parameter-free partition between moistening and precipitation in the Kuo scheme. *Mon. Wea. Rev.*, **113,** 405–407.

Gray, W. M., E. Ruprecht and R. Phelps, 1975: Relative humidity in tropical weather systems. *Mon. Wea. Rev.*, **103,** 685–690.

Hack, J. J., and W. H. Schubert, 1980: The role of convective-scale processes in tropical cyclone development. Dept. of Atmos. Sci. Pap. No. 330, Colorado State University, Ft. Collins, CO, 206 pp.

——, and ——, 1981: Lateral boundary conditions for tropical cyclone models. *Mon. Wea. Rev.*, **109,** 1404–1420.

Hobgood, J. S., 1986: A possible mechanism for the diurnal oscillations of tropical cyclones. *J. Atmos. Sci.*, **43,** 2901–2922.

Jones, R. W., 1980: A three-dimensional tropical cyclone model with release of latent heat by the resolvable scales. *J. Atmos. Sci.*, **37,** 930–938.

Jordan, C. L., 1958: Mean soundings for the West Indies area. *J. Meteor.*, **15,** 91–97.

Jorgensen, D. P., 1984: Mesoscale and convective-scale characteristics of mature hurricanes. Part II: Inner core structure of hurricane Allen (1980). *J. Atmos. Sci.*, **41,** 1287–1311.

Klemp, J. B., and R. B. Wilhelmson, 1978: The simulation of three-dimensional convective storm dynamics. *J. Atmos. Sci.*, **35,** 1070–1096.

Kondo, J., 1975: Air–sea bulk transfer coefficients in diabatic conditions. *Bound.-Layer Meteor.*, **9,** 91–112.

Kuo, H. L., 1965: On formation and intensification of tropical cyclones through latent heat release by cumulus convection. *J. Atmos. Sci.*, **22,** 40–63.

——, 1974: Further studies of the parameterization of the influence of cumulus convection on large-scale flow. *J. Atmos. Sci.*, **31,** 1232–1240.

Kurihara, Y., 1975: Budget analysis of a tropical cyclone simulated in an axisymmetric numerical model. *J. Atmos. Sci.*, **32,** 25–59.

——, and R. E. Tuleya, 1974: Structure of a tropical cyclone developed in a three-dimensional numerical simulation model. *J. Atmos. Sci.*, **31,** 893–919.

——, and ——, 1981: A numerical simulation study on the genesis of a tropical storm. *Mon. Wea. Rev.*, **109,** 1629–1653.

Manabe, S., J. Smagorinski and R. F. Strickler, 1965: Simulated climatology of a general circulation model with a hydrologic cycle. *Mon. Wea. Rev.*, **93,** 769–798.

Ooyama, K. V., 1982: Conceptual evolution of the theory and mod-

eling of the tropical cyclone. *J. Meteor. Soc. Japan,* **60,** 369–380.

Riehl, H., and J. Malkus, 1961: Some aspects of hurricane Daisy, 1958. *Tellus,* **13,** 181–213.

Rosenthal, S. L., 1978: Numerical simulation of tropical cyclone development with latent heat release by the resolvable scales I: Model description and preliminary results. *J. Atmos. Sci.,* **35,** 258–271.

Rotunno, R., and K. A. Emanuel, 1987: An air–sea interaction theory for tropical cyclones. Part II: Evolutionary study using a non-hydrostatic axisymmetric numerical model. *J. Atmos. Sci.,* **44,** 542–561.

Schubert, W. H., J. J. Hack, P. L. Silva Dias and S. R. Fulton, 1980: Geostrophic adjustment in an axisymmetric vortex. *J. Atmos. Sci.,* **37,** 1464–1484.

Smagorinski, J., 1963: General circulation experiments with the primitive equations: I. The basic experiment. *Mon. Wea. Rev.,* **91,** 99–164.

Sundqvist, H., 1970: Numerical simulation of the development of tropical cyclones with a ten-level model. Part II. *Tellus,* **22,** 504–510.

Wada, M., 1979: Numerical experiments of the tropical cyclone by use of the Arakawa-Schubert parameterization. *J. Meteor. Soc. Japan,* **57,** 505–531.

Willoughby, H. E., J. A. Clos and M. G. Shoreibah, 1982: Concentric eye walls, secondary wind maxima, and the evolution of the hurricane vortex. *J. Atmos. Sci.,* **39,** 395–411.

——, H.-L. Jin, S. J. Lord and J. M. Piotrowicz, 1984: Hurricane structure and evolution as simulated by an axisymmetric, non-hydrostatic numerical model. *J. Atmos. Sci.,* **41,** 1169–1186.

Yamasaki, M., 1977: A preliminary experiment of the tropical cyclone without parameterizing the effects of cumulus convection. *J. Meteor. Soc. Japan.,* **55,** 11–31.